

Particle production and long-range correlations in p +Pb collisions with the ATLAS detector.

Alexander Milov on behalf of the ATLAS Collaboration

Department of Particle Physics and Astrophysics, Weizmann Institute of Science, 234 Herzl str., Rehovot 7610001, Israel

Abstract

The ATLAS experiment at the LHC has measured the centrality dependence of charged particle pseudorapidity distribution, charged particle spectra, and the two-particle correlations in p +Pb collisions at a nucleon-nucleon centre-of-mass energy of $\sqrt{s_{NN}}=5.02$ TeV. Charged particles were measured over $|\eta| < 2.7$ using the ATLAS detector tracking system. The p +Pb collision centrality was characterized by the total transverse energy deposited over the interval $3.2 < \eta < 4.9$ in the direction of the Pb-beam. Three different calculations of the number of participating nucleons, have been carried out using a standard Glauber initial state model as well as two Glauber-Gribov extensions. Charged particle multiplicities per participant pair, and the normalised charged particle spectra are found to vary in shape with η and also with the model, pointing to the importance of the fluctuating nature of nucleon-nucleon collisions in the modelling of the initial state of p +Pb collisions. The two particle correlation exhibits flow-like modulations for all centrality intervals and particle p_T .

Keywords: Heavy Ion Collisions, Centrality, Multiplicity, Spectra, Nuclear Modification Factor, Two-Particle Correlations

1. Introduction

Proton-lead collisions (p +Pb) at the Large Hadron Collider (LHC) provide an opportunity to probe the physics of the initial state of ultra-relativistic heavy ion collisions without obscuring effects of thermalization and collective evolution [1]. The LHC delivered its first p +Pb collisions at $\sqrt{s_{NN}}=5.02$ TeV in a short pilot run in September 2012. Over several hours ATLAS detector [2] collected an event sample with integrated luminosity of approximately $1 \mu\text{b}^{-1}$, assuming an input cross section for p +Pb collisions of 2.1b estimated using a p +Pb Glauber model.

This report reviews the results on the measurement of the charged particle production and correlations observed in p +Pb collisions at the LHC. For the first time the results are analysed as a function of centrality, which provides additional information for understanding the underlying physics. Results are presented for several centrality intervals characterised by the sum of transverse energy (ΣE_T^{Pb}) measured in the forward (Pb-going) section of the ATLAS calorimeter.

2. Centrality determination in p +Pb collisions

The geometry of nucleus-nucleus and proton-nucleus collisions can be studied using Glauber Monte Carlo model [4] that simulates interactions of incident nucleons using a semi-classical eikonal approximation. A modified version of the Glauber model, referred to as Glauber-Gribov, was implemented in the PHOBOS generator [3] to account for event-to-event fluctuations in the nucleon-nucleon cross section (σ_{NN}) [5–7]. The Glauber model uses a fixed inelastic cross section, which is assumed to be 70 mb in this measurement. The Glauber-Gribov extensions use the

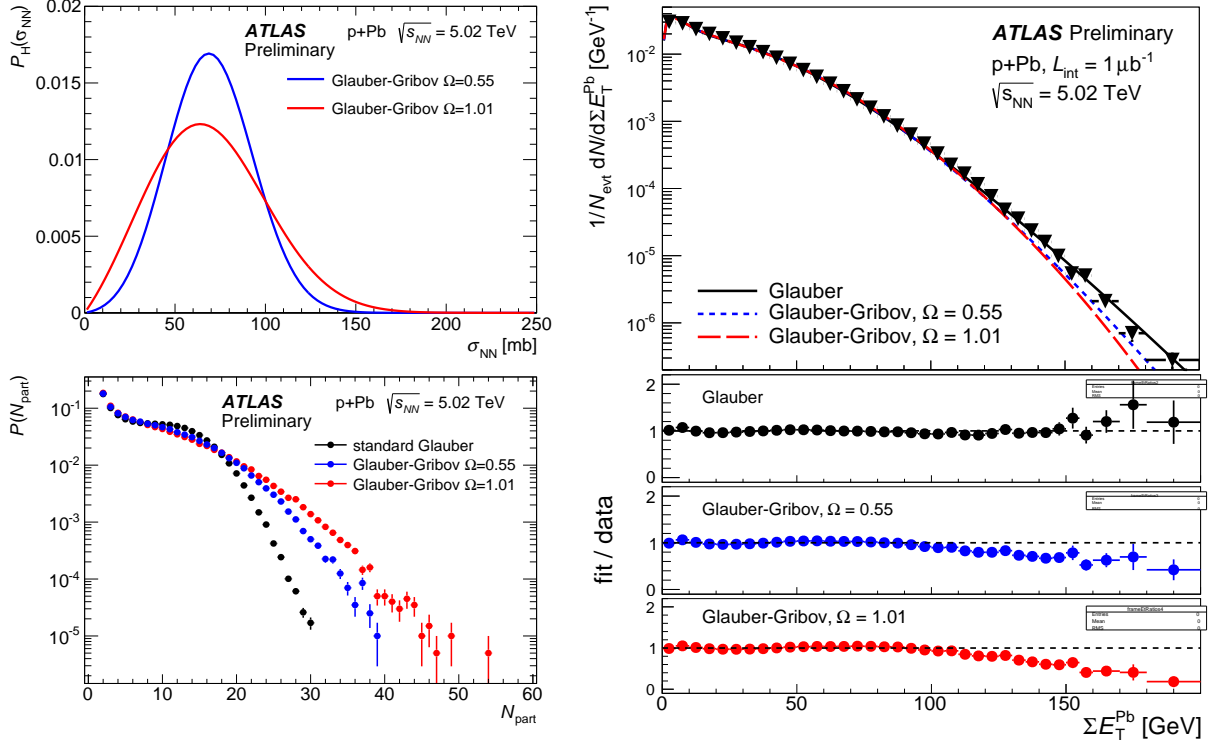


Figure 1. Top left: Glauber-Gribov probability distribution for per-nucleon cross section for $\Omega = 0.55$ and 1.01 . Lower left: The N_{part} distributions for the Glauber and Glauber-Gribov Monte Carlo models simulated 5.02 TeV $p+\text{Pb}$ collisions (1 million simulated events each). Top right: Comparison of the measured ΣE_T^{Pb} distribution to Glauber and Glauber-Gribov fits. Lower panels show ratios of the fits to the data distribution. Plots are from Ref. [8].

probability distribution of the total cross section shown in the upper left panel of Fig. 1. Parameter Ω defines the width of the total cross section probability distribution. The distribution of the number of nucleons participating in collision (N_{part}) for the Glauber and Glauber-Gribov Monte Carlo models are shown in the lower left panel of the figure. The Glauber-Gribov analysis was performed using both $\Omega = 0.55$ and 1.01 , motivated in Refs. [6, 7, 9, 10], in order to evaluate the sensitivity of the physics conclusions to the choice of Ω . For all three calculations, the lead nucleon density distribution was taken to be Woods-Saxon with radius and skin depth parameters, $R = 6.62$ fm and $a = 0.546$ fm respectively [11]. The Glauber-Gribov N_{part} distributions are much broader than the Glauber distribution due to σ_{NN} fluctuations in the Glauber-Gribov formulation.

The Wounded Nucleon (WN) model [12] is used to connect an experimentally measured ΣE_T^{Pb} distribution to the results of the Glauber or Glauber-Gribov Monte Carlo. For fixed N_{part} , the measured distribution can be obtained from the WN model as an n -fold convolution of the corresponding $p+p$ distribution, where n is equal to N_{part} . The $p+p$ distribution is taken from a full detector simulation based on PYTHIA8 (and verified with PYTHIA6) [13] at $\sqrt{s}=5.02$ TeV. The results of the simulation were compared at the detector level to the measured distributions at lower $\sqrt{s}=2.76$ TeV and higher 7 TeV $p+p$ energies. The distributions are approximated by the gamma distribution form $\text{gamma}(k, \theta)$. The n -fold convolution of the gamma distribution is straightforward to implement analytically, however, to obtain the best agreement between the data and the models the parameters of the distributions were assumed to be dependent on the number of participants: $k(N_{\text{part}})$, $\theta(N_{\text{part}})$. The results of the fit using the Glauber or Glauber-Gribov Monte Carlo to reproduce the measured ΣE_T^{Pb} distribution are shown in the right panel of Fig. 1. The fit allows to associate the energy interval of ΣE_T^{Pb} to the $\langle N_{\text{part}} \rangle$ from the Glauber model.

3. Charged particle multiplicity

The measurement of the charged particle multiplicity was performed using only the pixel detector to maximize the efficiency for reconstructing charged particles with low-transverse momenta [8]. Two approaches are used in this analysis. The first is the two-point tracklet method commonly used in heavy ion collision experiments [14–16]. The second method uses “pixel tracks”, obtained by applying the full track reconstruction algorithm to only the pixel detector. The pixel tracking is less efficient than the tracklet method, but provides measurements of particle p_T . The $dN_{ch}/d\eta$ measured using pixel tracks is used as a validation of the measurement with the two-point tracklets. The tracklet method used in two different implementations and the pixel track methods agree to each other. The first results on the $dN_{ch}/d\eta$ measured in different centrality intervals are shown in Fig. 2.

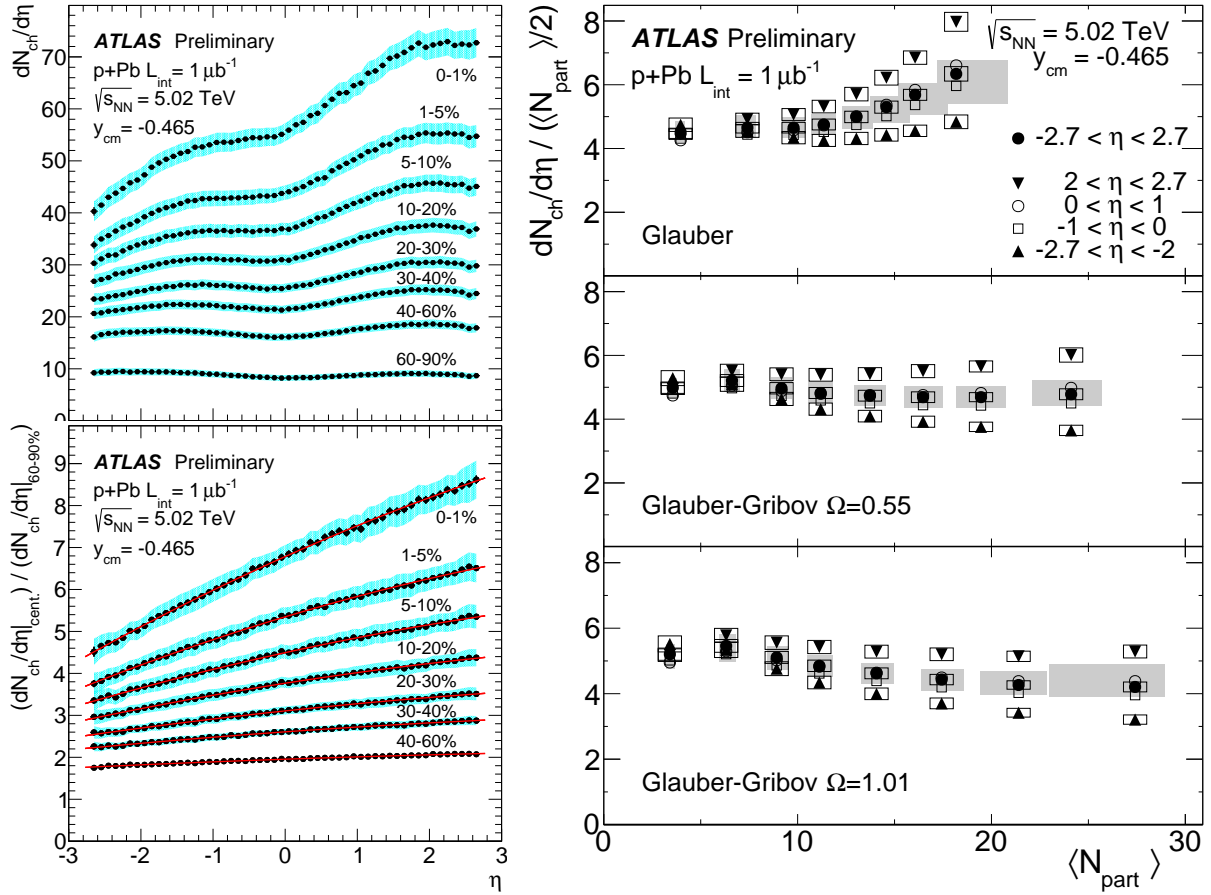


Figure 2. Top left: Charged particle density $dN_{ch}/d\eta$ measured in different centrality intervals. Statistical uncertainties, shown with vertical bars, are typically smaller than the marker size. Colour bands show the systematic uncertainty. Bottom left: The $dN_{ch}/d\eta$ measured in different centrality classes divided by $dN_{ch}/d\eta$ measured in the peripheral (60-90%) centrality interval. Lines show the results of second order polynomial fits to the data points. Right panels: Charged particle density $dN_{ch}/d\eta$ per pair of participants measured in different η ranges, as a function of $\langle N_{part} \rangle$ obtained using three initial state models. The bands shown with thin lines represent the systematic uncertainty of the $dN_{ch}/d\eta$ measurement, the shaded bands indicate the total systematic uncertainty including the uncertainty on $\langle N_{part} \rangle$. Statistical uncertainties, shown with vertical bars are typically smaller than the marker size. Plots are from Ref. [8].

The upper left panel of Figure 2 presents the charged particle pseudorapidity density for p +Pb collisions at $\sqrt{s_{NN}} = 5.02$ TeV over the pseudorapidity interval $|\eta| < 2.7$ in eight centrality intervals from the 0–1% most central to 60–90% most peripheral. In the most peripheral collisions the $dN_{ch}/d\eta$ has a characteristic shape which is similar to a symmetric double-peak structure, seen in proton-proton collisions [17, 18]. In more central collisions, the shape of $dN_{ch}/d\eta$ becomes progressively more asymmetric, with more particles produced in the Pb-going direction than in the proton-going direction.

To investigate further the centrality evolution, the distributions in the various centrality intervals are divided by the distribution measured in 60–90% centrality. The ratios are shown in the lower left panel of the figure. The double peak structure seen in the upper panel disappears in the ratios. The ratios are observed to grow nearly linearly with pseudorapidity, with a slope that increases from peripheral to central collisions. The ratios are well approximated with a second order polynomial fitted to data points.

The right panel of the figure shows $dN_{\text{ch}}/d\eta$ per participant pair for the most central and most peripheral intervals of centrality measured as a function of η for three different implementations of the Glauber model explained in Sec. 2. The results for the most peripheral (60–90%) centrality interval shown with circles, reside approximately at the same magnitude in all three panels. In the region $-1 < \eta < 0$ this magnitude is consistent with the ($\propto s^{0.10}$) approximation of $dN_{\text{ch}}/d\eta$ in inelastic $p+p$ collisions, shown in Fig. 1 of Ref. [19]. The magnitude of $dN_{\text{ch}}/d\eta$ per participant pair strongly depends on pseudorapidity, consistent with the findings at RHIC [20], and also on the model used to calculate $\langle N_{\text{part}} \rangle$.

4. Nuclear modification factor

The ATLAS experiment at the LHC measures the differential invariant p_T yields for charged particles in $p+\text{Pb}$ collisions at $\sqrt{s}=5.02$ TeV [21]. The spectra are reconstructed over the available pseudorapidity interval $|\eta| < 2.5$ in the same centrality intervals as the multiplicity measurement. The spectra are studied as a function of the centre-of-mass rapidity $y^* = y + 0.465$, calculated assuming the particle having the pion mass, and then corrected for the actual mass based on the Monte-Carlo simulations. The fully corrected charged particle production cross section as a function of p_T are also measured in $p+p$ collisions at the centre of mass energies of $\sqrt{s}=2.76$ TeV and 7 TeV. The differential cross sections at the two energies are interpolated to obtain the differential cross section at $\sqrt{s}=5.02$ TeV used to derive the nuclear modification factor (R_{pPb}). The definition of the R_{pPb} can be found in [21].

Figure 3 shows R_{pPb} as a function of p_T . Three panels in each column correspond to the most central (upper

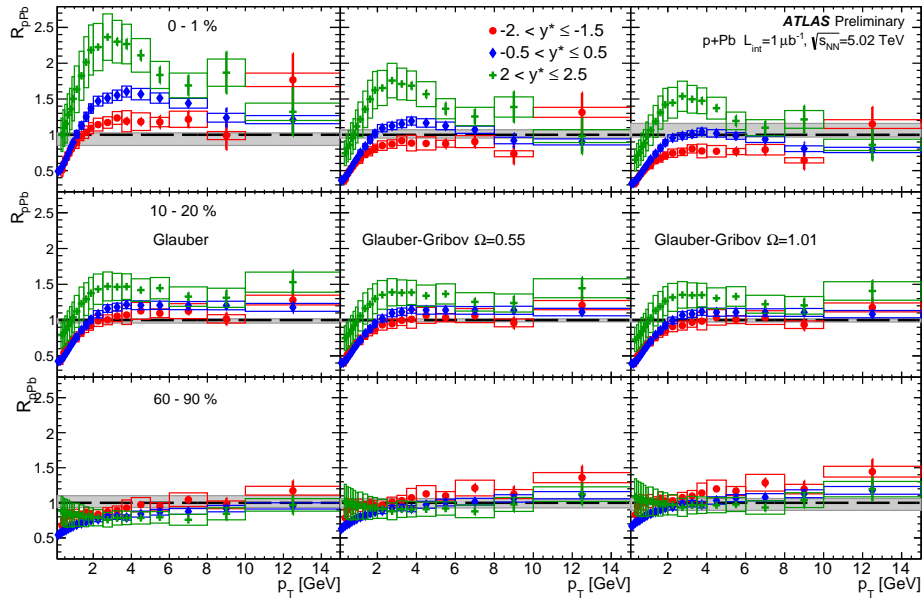


Figure 3. The R_{pPb} measured for 0–1% most central collisions (top panels) 10–20% centrality interval (middle panels) and 60–90% centrality interval (lower panels). The data points are shown for 3 different rapidity intervals indicated in the legend. The columns correspond to the Glauber model (left), Glauber-Gribov model with $\Omega = 0.55$ (middle), and Glauber-Gribov model with $\Omega = 1.01$ (right) calculations. The grey box on each axis reflects the systematic uncertainty associated with the centrality interval and with the model assumption. Systematic uncertainties due to the analysis of the spectra are plotted with boxes at each point. Vertical bars are the statistical uncertainty of the measurement. Plot is from Ref. [21].

panels), mid-central (middle panels) and most peripheral (lower panels) centrality intervals. Each panel has three sets

of points corresponding to different y^* intervals for R_{pPb} . The three columns show the results from the three different geometrical models: Glauber model (left), Glauber-Gribov model with $\Omega = 0.55$ (middle), and Glauber-Gribov model with $\Omega = 1.01$ (right).

Figure 3 shows that the magnitude of the peak at $p_T=2-4$ GeV, relative to the almost constant behaviour above 8 GeV, depends not only on centrality, but also on rapidity. It increases with increasing y^* (i.e. moving farther toward the rapidity of the Pb nucleus), as observed in the upper and middle panels of the figure. The rapidity intervals in the proton beam direction (negative y^*) show a smaller peak compared to the rapidity interval in the Pb beam direction. The magnitude of the constant region also depends on rapidity. The nuclear modification factors in the constant region ($p_T > 8$ GeV) show much less variation over the measured rapidity region for all centralities. The limited statistics of the pilot $p+Pb$ run precludes conclusive statements about the R_{pPb} behaviour as a function of y^* in the high p_T part of the spectrum.

5. Charged particle correlations

The ATLAS experiment measured the strength of the long-range two-particle correlations in $p+Pb$ collisions at $\sqrt{s}=5.02$ TeV quantified by the per-trigger yield, $Y(\Delta\phi)$ [22]. The yields are integrated over relative differences $2 < |\Delta\eta| < 5$ between the “trigger particle” (a) and associated particle (b) and the background is subtracted based on the zero-yield-at-minimum (ZYAM) method.

$Y(\Delta\phi)$ distributions for peripheral and central events and their difference are shown as a function of $|\Delta\phi|$ in the left two columns of Fig. 4 for various p_T^a ranges with $0.5 < p_T^b < 4$ GeV. The difference is observed to be nearly

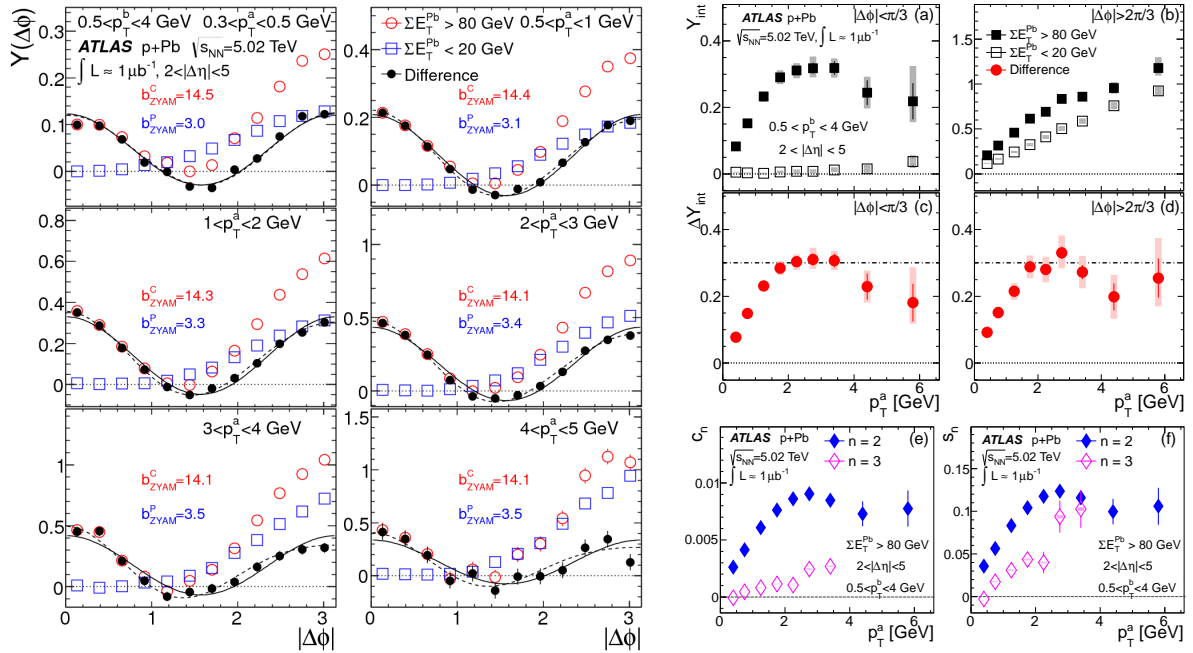


Figure 4. Left panels: Distributions of per-trigger yield in the peripheral and the central event activity classes and their differences (solid symbols), for different ranges of p_T^a and $0.5 < p_T^b < 4$ GeV, together with functions $a_0 + 2a_2 \cos 2\Delta\phi$ (solid line) and $a_0 + 2a_2 \cos 2\Delta\phi + 2a_3 \cos 3\Delta\phi$ (dashed line) obtained via a Fourier decomposition. The values for the ZYAM-determined pedestal levels are indicated on each panel for peripheral (b_{ZYAM}^P) and central (b_{ZYAM}^C) ΣE_T^{Pb} bins. Right panels: Integrated per-trigger yields, Y_{int} , vs p_T^a for $0.5 < p_T^b < 4$ GeV in peripheral and central events, on the (a) near-side and (b) away-side. The panels (c) and (d) show the difference, ΔY_{int} . Panels (e) and (f) show the p_T dependence of c_2 , c_3 and s_2 , s_3 . The error bars and shaded boxes represent the statistical and systematic uncertainties, respectively. Plots are from Ref. [22].

symmetric around $\Delta\phi = \pi/2$. To illustrate this symmetry, the $Y(\Delta\phi)$ distributions in Fig. 4 are overlaid with the

function symmetric around $\pi/2$ (solid curve), indicating that the long-range component of the two-particle correlations can be approximately described by a recoil contribution plus a $\Delta\phi$ -symmetric component.

The near-side and away-side yields, integrated respectively over $|\Delta\phi| \leq \pi/3$ and $|\Delta\phi| > 2\pi/3$ (Y_{int}), and the differences between these integrated yields in central and peripheral events (ΔY_{int}), are shown in the right two columns of Fig. 4 as a function of p_T^a . The yields are shown separately for two ΣE_T^{Pb} ranges in panels (a) and (b) and the differences are shown in panels (c) and (d). Qualitatively, the differences have a similar p_T^a dependence and magnitude on the near-side and away-side; they rise with p_T^a and reach a maximum around 3–4 GeV.

The relative amplitude of the $\cos(n\Delta\phi)$ modulation of $Y(\Delta\phi)$, (c_n) can be estimated from the fits shown in the left two columns as explained in Ref. [22]. Panel (e) of Fig. 4 shows c_2 and c_3 as a function of p_T^a for $0.5 < p_T^b < 4$ GeV. The value of c_2 is much larger than c_3 and exhibits a behaviour similar to $Y(\Delta\phi)$ at the near-side and away-side. The values of c_n can be converted into an estimate of s_n , the average n -th Fourier coefficient of the event-by-event single-particle ϕ -distribution. The $s_2(p_T^a)$ values obtained this way exceed 0.1 at ~ 2 –4 GeV, as shown in Fig. 4(f). The transverse momentum dependence of s_2 and s_3 is similar to that observed for long-range correlations in Pb+Pb collisions [23, 24].

6. Summary

This report presents the measurements of the centrality dependence of the charged particle pseudorapidity distribution, $dN_{\text{ch}}/d\eta$, R_{pPb} and two particle correlations in p +Pb collisions as a function of p_T at a nucleon-nucleon centre-of-mass energy of $\sqrt{s_{NN}} = 5.02$ TeV collected by the ATLAS detector using data sample of the pilot run commenced by the LHC in September 2012. The centrality is characterized using a forward calorimeter covering $3.1 < \eta < 4.9$ in the Pb-going direction. The average number of participants in each centrality interval, $\langle N_{\text{part}} \rangle$, was estimated with the Glauber and Glauber-Gribov Monte Carlo models using the simulated response of the ATLAS forward calorimeter in Pb-going direction.

The $dN_{\text{ch}}/d\eta$ distribution, presented over the pseudorapidity range $-2.7 < \eta < 2.7$ evolve gradually with centrality from an approximately symmetric shape in the most peripheral collisions to a highly asymmetric distribution in the most central collisions. The ratios of $dN_{\text{ch}}/d\eta$ distributions in different centrality intervals to the $dN_{\text{ch}}/d\eta$ in the most peripheral interval are approximately linear in η with a slope that is strongly dependent on centrality. The nuclear modification factor, R_{pPb} , is measured as a function of the centre-of-mass rapidity in the range $-2 < y^* < 2.5$ and for transverse momentum $0.1 < p_T < 22$ GeV. The reference p + p cross-section is obtained by interpolating the measurements performed at $\sqrt{s}=2.76$ TeV and 7 TeV. The shape and the magnitude of the R_{pPb} was found to have a strong rapidity dependence. Both the N_{part} dependence of $dN_{\text{ch}}/d\eta/(\langle N_{\text{part}} \rangle/2)$ and the R_{pPb} are sensitive to the Glauber modeling, especially in the most central collisions.

The two-particle correlation function measured in p +Pb collisions clearly shows ridge structures resembling those observed in Pb+Pb collisions and suggesting that collective flow may also be present in p +Pb collisions. The flow interpretation of the p +Pb data is also supported by results from multi-particle azimuthal correlation measurements [25].

The work of the author is supported by the Israel Science Foundation (grant 710743).

References

- [1] L. P. Csernai, J. Kapusta, L. D. McLerran, Phys. Rev. Lett. 97 (2006) 152303.
- [2] ATLAS Collaboration, The ATLAS Experiment at the CERN Large Hadron Collider, JINST 3 (2008) S08003.
- [3] M. L. Miller, K. Reygers, S. J. Sanders, P. Steinberg, Ann. Rev. Nucl. Part. Sci. 57 (2007) 205–243.
- [4] B. Alver, M. Baker, C. Loizides, P. Steinberg, arXiv:0805.4411.
- [5] H. Heiselberg, G. Baym, B. Blaettel, L. Frankfurt, M. Strikman, Phys. Rev. Lett. 67 (1991) 2946–2949.
- [6] V. Guzey, M. Strikman, Phys. Lett. B633 (2006) 245–252.
- [7] M. Alvioli, M. Strikman, Phys. Lett. B722 (2013) 347–354.
- [8] ATLAS Collaboration, ATLAS-CONF-2013-096.
- [9] G. Antchev, et al., Phys. Rev. Lett. 111 (2013) 012001.
- [10] A. Donnachie, P. Landshoff, Phys. Lett. B296 (1992) 227–232.
- [11] H. De Vries, C. De Jager, C. De Vries, Atom. Data Nucl. Data Tabl. 36 (1987) 495–536.
- [12] A. Bialas, M. Bleszynski, W. Czyz, Nucl. Phys. B111 (1976) 461.
- [13] ATLAS Collaboration, ATLAS-PHYS-PUB-2011-009.
- [14] ATLAS Collaboration, Phys. Lett. B710 (2012) 363–382.

- [15] K. Adcox, et al., Phys. Rev. Lett. 86 (2001) 3500–3505.
- [16] B. Alver, et al., Phys. Rev. C83 (2011) 024913.
- [17] ATLAS Collaboration, New J. Phys. 13 (2011) 053033.
- [18] ATLAS Collaboration, Phys. Lett. B688 (2010) 21–42.
- [19] ALICE Collaboration, Phys. Rev. Lett. 110 (2013) 032301.
- [20] B. Back, et al., Phys. Rev. C72 (2005) 031901.
- [21] ATLAS Collaboration, ATLAS-CONF-2013-107.
- [22] ATLAS Collaboration, Phys. Rev. Lett. 110 (2013) 182302.
- [23] ATLAS Collaboration, Phys. Rev. C86 (2012) 014907.
- [24] CMS Collaboration, Eur. Phys. J. C 72 (5) (2012) 1–26.
- [25] ATLAS Collaboration, Phys. Lett. B725 (2013) 60–78.